Dynamics of Hydrogen−Deuterium Exchange in *Chlamydomonas* Centrin†

Mildred Ortiz,‡ Zuleika Sanoguet,‡ Haitao Hu,§ Walter J. Chazin,§ Cynthia T. McMurray,|| Jeffrey L. Salisbury,⊥ and Belinda Pastrana-Rios*,‡

Department of Chemistry and Center for Protein Structure Function and Dynamics, University of Puerto Rico, Mayagüez Campus, P.O. Box 9019, Mayagüez, Puerto Rico 00681-9019, Departments of Biochemistry and Physics and Center for Structural Biology, Vanderbilt University, Nashville, Tennessee 37232-0146, and Department of Molecular Pharmacology and Experimental Therapeutics and Department of Biochemistry and Molecular Biology, Mayo Clinic and Foundation, Rochester, Minnesota 55905

Received July 21, 2004; Revised Manuscript Received November 11, 2004

ABSTRACT: *Chlamydomonas reinhardtii* centrin is a 169-amino acid residue calcium binding protein belonging to the EF-hand protein superfamily. Centrin is associated with the microtubule organizing center (MTOC) in all eukaryotes, and in *Chlamydomonas*, centrin is a component of the flagellar basal body apparatus. Recombinant full-length centrin, calmodulin, and terminal domain fragments [Ccen-N (residues 1−94) and Ccen-C (residues 99−169)] were used to examine hydrogen−deuterium (H → D) exchange dynamics using combined attenuated total reflectance (ATR) Fourier transform-infrared (FT-IR) spectroscopy, curve fit, and two-dimensional correlation analysis. Analysis of the Ccen-N and Ccen-C fragments allowed separation of domain specific solvent exchange events and together with analysis of the full-length proteins provides novel insight into domain accessibility to the aqueous environment and the internal dynamics of the protein.

Centrin is an acidic, low-molecular weight protein ($M_r \sim$ 20 000) that belongs to the EF-hand superfamily of calcium binding proteins (*1*−*4*). This calcium binding protein is one of ∼350 proteins that are unique to eukaryotic cells (*5*). It was first identified as a major component of the fibers that link the nucleus to the flagellar apparatus in flagellated unicells (*6*) and, later, shown to be a ubiquitous component of centrioles and mitotic spindle poles (*7*, *8*). CDC31 (a yeast homologue), *Chlamydomonas reinhardtii*, human, and mice centrins have been shown to have an essential role in the duplication and separation of the microtubule organizing center (MTOC)[1] in their respective cells (*7*, *9*−*18*). Furthermore, Marshall and co-workers (*19*, *20*) have carried out genetic studies in *C. reinhardtii*, resulting in the implication of centrin's role in the biogenesis of centrioles.

Structurally, centrin contains four helix−loop−helix motifs or EF-hands, each of which has the potential to bind one calcium atom (*1*−*3*). The level of sequence identity shared between centrin and calmodulin is ∼50%, suggesting similar secondary structure (Figure 1). Like calmodulin, the helix−loop−helix motif in centrin is the most conserved feature in the protein. The residues involved in the Ca^{2+} coordination for both proteins are shown in Figure 1C. The affinity of centrin for calcium in the C-terminal domain is lower than the affinity for the N-terminal domain or calmodulin (*1*, *3*, *4*). Upon closer inspection, centrin contains a positively charged amino-terminal end and an aromatic residue located at the carboxy terminus, both of which are lacking in the calmodulin sequence. *C. reinhardtii* centrin has been characterized in the presence and absence of cations using FT-IR (*21*, *22*), CD (*3*, *21*, *23*), and NMR (*3*, *4*) spectroscopies. Nuclear magnetic resonance (NMR) spectroscopic studies of centrin indicated that the central helix is highly mobile in solution and acts as a flexible linker (*3*, *4*). Thus, centrin contains two structurally independent domains (Ccen-N and Ccen-C) that each contain a pair of EF-hand motifs (*4*). A 60% helical content for holocentrin has been determined by FT-IR (*21*, *22*), CD (*3*, *21*, *23*), and NMR (*3*). Self-association was observed for centrin in the presence and absence of cations, but in the presence of calcium and magnesium, less than 10% self-association was observed (refs *21* and *22* and manuscript in preparation).

Fourier transform infrared (FT-IR) spectroscopy (*24*, *25*) has shown great promise for the study of conformational

† This project is supported by NIH-SCORE Grant 5-S06GM08103 (B.P.-R.) and RO1-GM40120 (W.J.C.), the University of Puerto Rico, and Vanderbilt University.

* To whom correspondence should be addressed: Department of Chemistry, University of Puerto Rico, Mayagüez Campus, P.O. Box 9019, Mayagüez, PR 00681-9019. Phone: (787) 265-6520. Fax: (787) 265-3849. E-mail: belinda@hpcf.upr.edu.

‡ University of Puerto Rico.

§ Vanderbilt University.

|| Department of Molecular Pharmacology and Experimental Therapeutics, Mayo Clinic and Foundation.

⊥ Department of Biochemistry and Molecular Biology, Mayo Clinic and Foundation.

[1] Abbreviations: FT-IR, Fourier transform-infrared; H → D, hydrogen−deuterium; ATR, attenuated total reflection; 2DCOS, two-dimensional correlation spectroscopy; MTOC, microtubule organizing center; CaM, calmodulin; Ccen, *C. reinhardtii* centrin; Ccen-N, *C. reinhardtii* centrin amino-terminal domain fragment comprised of 99 residues; Ccen-C, *C. reinhardtii* centrin carboxy-terminal domain fragment comprised of 77 residues; IPTG, isopropyl β-D-thiogalactopyranoside; TOF, time-of-flight mass spectrometry; EDTA, ethylenediaminetetraacetic acid, tetrasodium salt; EGTA, ethylene glycol bis(aminoethyl ether)tetraacetic acid.

10.1021/bi0484419 CCC: $30.25
Published on Web 01/28/2005

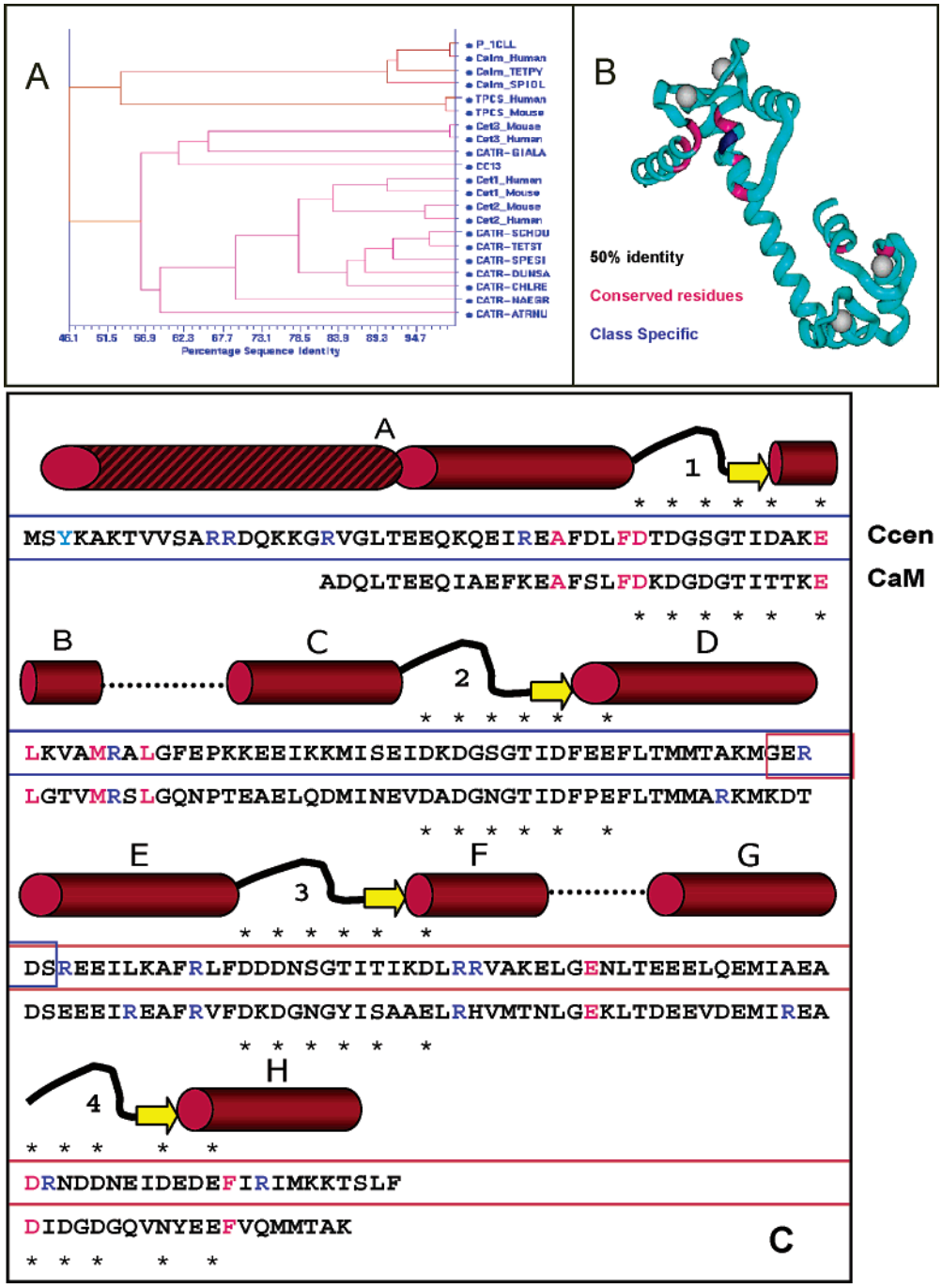

FIGURE 1: (A) Evolutionary trace and (B) structural homology for calmodulin, troponin C, and centrin generated using NCBI-BLAST, ClustalW, and Binding Site from Insight II (Accelrys). (C) Sequence alignment of *Chlamydomonas* centrin and human calmodulin along with a schematic representation of CaM structural motifs. The red striped helix is the proposed secondary structure for the amino-terminal end of Ccen. Residues have been color-coded to show the Arg (blue) and Tyr (cyan) residues within each sequence and to depict the conserved residues (purple). Furthermore, the asterisk denotes the Ca^{2+} coordination site for the canonical and noncanonical binding site. Finally, the terminal domain fragments Ccen-N and Ccen-C within the centrin sequence have been boxed in blue and red, respectively.

changes in proteins (*21*, *22*, *26*, *27*). The exchange of amide protons with D_2O has become increasingly important as a means of characterizing the structure and dynamics of proteins (*28*−*31*). A common technique used in these studies of hydrogen−deuterium (H → D) exchange is known as attenuated total reflectance (ATR) FT-IR spectroscopy (*28*, *29*) due to the ease of sample preparation for this type of experiment. For spectral analysis, two-dimensional correlation has proven to be useful in enhancing spectral resolution and determining the order of events during a perturbation (*21*, *26*, *27*, *29*, *32*−*34*).

We have used ATR FT-IR, two-dimensional correlation analysis, and a curve fitting approach to resolve the dynamic molecular events that occur upon H → D exchange. H → D exchange of labile amide protons and other exchangeable protons that have limited accessibility to their aqueous environment is dependent on the structural properties of the protein. The advantage of this study is that H → D exchange does not perturb the protein's secondary structure (*29*, *35*).

A comparative study of full-length centrin with its domain fragments can provide further understanding of the molecular dynamics of these domains in holocentrin. The amide I′ band

is very sensitive to backbone conformation and is able to distinguish several structural domains (*21*, *22*, *24*−*27*, *34*−*36*). Routinely, spectral band intensity changes are observed for the amide II band (1500−1600 cm^{-1}) and amide II′ band (1400−1500 cm^{-1}) spectral regions upon exposure of the protein to D_2O vapor. The concomitant band intensity changes are indicative of H → D exchange. In addition, to amide vibrational modes which provide secondary structure information, the arginine and the tyrosine side chain modes (*37*) have exchangeable protons that can provide information about the extent of solvation in their immediate surroundings, thus acting as an internal probe. This single tyrosine residue present only in the amino-terminal (helix A) domain of centrin would provide insight about the solvation of this helix with respect to the other helical motifs present in the structure. Conversely, the H → D exchange observed for the arginine residues in Ccen-C can be directly related to calmodulin.

The biophysical study of centrin, its terminal fragments, and calmodulin H → D exchange discussed herein provides an understanding of solvation dynamics in centrin. These in vitro studies are the groundwork for comparison of centrin and centrin complexes with other interacting proteins and peptides such as Kar1p, Mps3p, and, most recently discovered, sfi1p, involved in the duplication and assembly of spindle pole body (SPB) (*13*, *16*, *17*). Future H → D exchange dynamic studies will involve the study of these complexes to provide insight into the biochemical changes through which centrin plays a role in the process of cell division.

METHODS

Recombinant *Chlamydomonas* centrin was overexpressed using a pt7-5 plasmid construct in *Escherichia coli* BL21-λDE_3. Bacterial cells were grown in 2XYT medium using a Bioflo 3000 fermentor equipped with a 5 L vessel. Cell growth was monitored with OD readings at 500 nm, and protein expression was induced with 0.5 mM ITPG (isopropyl β-D-thiogalactopyranoside) when cells reached the log phase. Typically, the 5 L bacterial culture yields ∼70 g of pellet. Details of the routine isolation and purification procedure followed in our laboratory are described by Pastrana-Rios et al. (*21*). Briefly, the solution was passed through an affinity column containing phenyl-Sepharose CL-4B. This column was equilibrated with a buffer containing 50 mM Tris, 0.5 mM EDTA, 0.5 M NaCl, 4.0 mM $MgCl_2$, 2.0 mM $CaCl_2$, 0.1% IGEPAL, and 0.04% NaN_3. *Chlamydomonas* centrin eluted with an elution buffer that contained 50 mM Tris, 0.5 mM EDTA, 5.0 mM EGTA, 0.5 M NaCl, 4.0 mM $MgCl_2$, and 0.04% NaN_3. Fractions containing full-length centrin that were identified through SDS−PAGE, the Bradford assay, and Western blot analysis were pooled, concentrated, and dialyzed. A second chromatography using an anion exchange column with a salt gradient was performed to elute the desired protein with an estimated purity of 99%. Fractions collected were analyzed through SDS−PAGE and the Bradford assay. Purified centrin was subjected to time-of-flight or MALDI mass spectroscopy and partial amino acid sequencing to verify its purity and identity. Human calmodulin was purchased from Calbiochem and used without further purification.

The recombinant terminal domain fragments Ccen-N and Ccen-C were generated from bacterial expression and subsequent isolation as described previously (*4*). These domains were also analyzed by MALDI MS to ensure purity.

For sample preparation, dialysis against 16 mM Hepes, 50 mM NaCl, 2 mM $CaCl_2$, and 2 mM $MgCl_2$ (pH 7.4) using a dialysis membrane (Spectrum Laboratories Inc.) cutoff of 100 Da (Ccen-N and Ccen-C) and 5 kDa (full-length centrin) was carried out. All of the buffers and salts were purchased from Sigma-Aldrich and used without further purification. H_2O was deionized with 18 Ω, and D_2O (99 at. % D) was purchased from Cambridge Isotopes Laboratories, Inc.

For these experiments, we used an FT-IR Mattson Infinity Series spectrophotometer equipped with an ATR accessory from Thermo Electron Corp. comprised of a horizontal ZnSe crystal with a 45° incident angle and an HgCdTe (MCT) detector. Typically, 0.5−1 mg of recombinant protein or terminal domain fragment solution was spread over the ATR crystal. The sample was purged with dry air until a dry film was obtained after ∼1 h, and spectral acquisition was initiated. Typically, 512 scans were taken, apodized with a triangular function, and Fourier transformed to provide a resolution of 4 cm^{-1} with the data encoded every 2 cm^{-1}. Spectra were collected until no further changes were observed within the absorption pattern.

Data obtained from FT-IR were processed with Grams (Galactic Industries) to introduce baseline correction into the collected spectra within the spectral region that was studied (1510−1710 cm^{-1}).

Two-dimensional analysis FT-IR correlation analysis was performed with MathCad 2000 Professional (MathSoft, Inc.). Further analysis of spectra for curve fitting was performed with Grams. The plots of the spectra were created with Origin 6 pro (MicroCal, Inc.).

RESULTS

H → D Exchange. This experiment allows for the study of exchangeable protons in proteins. Typical spectra acquired for full-length *Chlamydomonas* centrin and human calmodulin in the spectral region of 1380−1710 cm^{-1} are shown in panels A and B of Figure 2, respectively. The amide I band shifts to lower wavenumber, from 1649.5 to 1645.6 cm^{-1} and from 1648 to 1641 cm^{-1} for centrin and calmodulin, respectively. The amide II band (∼1576 cm^{-1}) shoulder at 1550 and 1547 cm^{-1} decreases in intensity for centrin and calmodulin, respectively, while the amide II′ band at 1450 and 1440 cm^{-1} concomitantly increases in intensity for centrin and calmodulin, respectively. Two-dimensional correlation analyses were carried out within the spectral region of 1400−1700 cm^{-1} for centrin and 1380−1710 cm^{-1} for calmodulin are shown in panels C and E and panels D and F of Figure 2 for the synchronous and asynchronous plots, respectively. Briefly, the peaks observed on the diagonal of the synchronous plot (Figure 2B) are called auto peaks and represent the vibrational modes that are been perturbed by the H → D exchange. Assignments of these peaks are as follows: the turn or loop (1675 cm^{-1}), the α-helix (1640 and 1650 cm^{-1}), the amino terminus (1560 cm^{-1}), the arginine modes (1570 and 1610 cm^{-1}), the N−H deformation mode (∼1550 cm^{-1}), the Tyr side chain mode

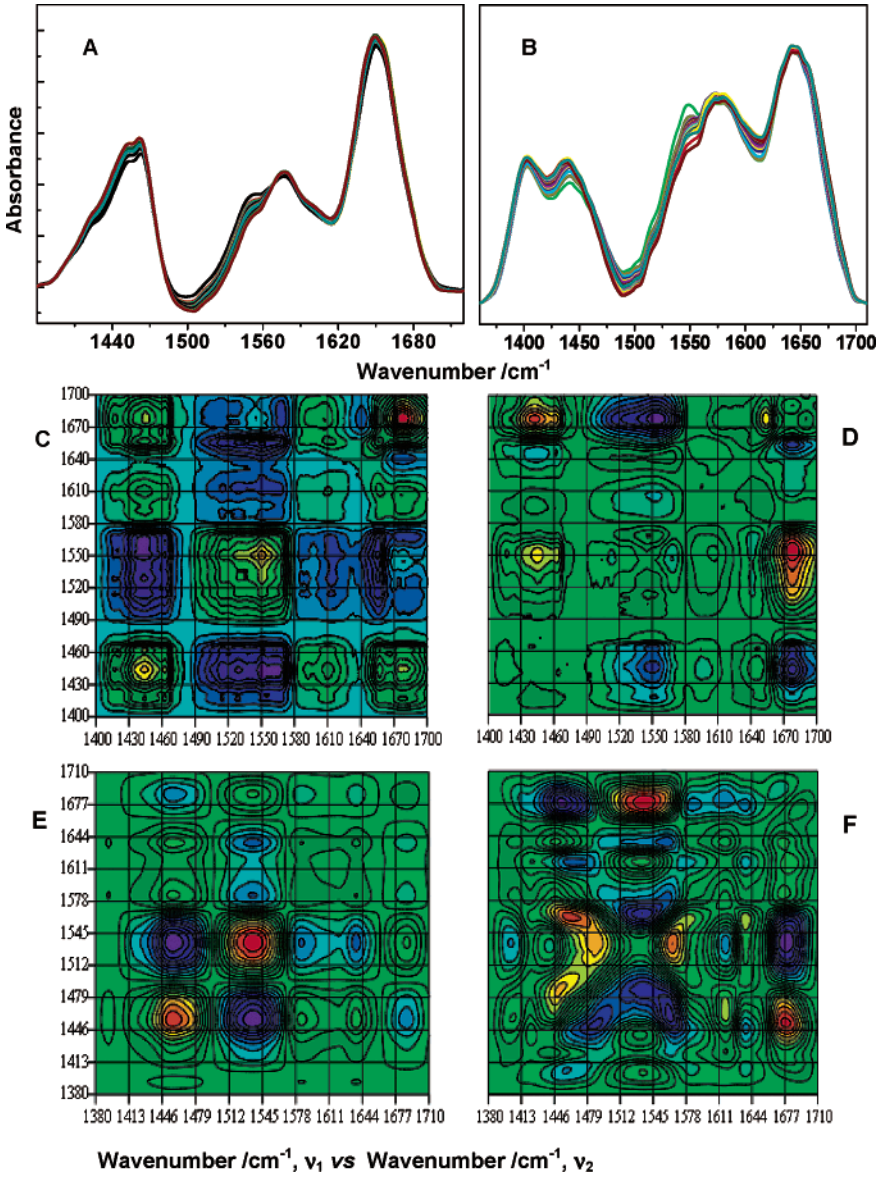

FIGURE 2: H → D exchange of full-length *Chlamydomonas* centrin and human calmodulin within the spectral region of 1380−1710 cm^{-1} at 20 °C shown as spectral overlays in panels A and B, respectively. The two-dimensional correlation analysis within the spectral region of 1380−1710 cm^{-1} for the time interval of 0−150 min: (C and E) synchronous plot and (D and F) asynchronous plot for Ccen and CaM, respectively. The spectral features that are shown are the overlapped amide I′ and amide I bands, side chain modes, and N−H deformation modes comprised of the amide II band, and the amide II′ band comprised of the N−D deformation mode.

[1510 cm^{-1} (D-form) and 1520 cm^{-1} (H-form)], and the N−D deformation mode (1450−1440 cm^{-1}). The asynchronous plot provides detailed information about the order of events upon perturbation of the centrin sample. One can compare the spectral data acquired for the full-length and terminal domain fragments within the spectral region of 1500−1700 cm^{-1} for centrin (Figure 3).

Dynamics of Exchange. The dynamics of exchange of centrin and calmodulin were compared in Figure 2. The synchronous plots for calmodulin (Figure 2D) show the greatest intensity change in the N−H and N−D deformation modes which are associated with the backbone amides. The H → D exchange for calmodulin occurs in the following order: loops and then arginine followed by the α-helix motifs. However, for centrin (Figure 2C), the intensity changes are in the loop and N−H and N−D deformation modes, thus suggesting different dynamics of solvent exchange was occurring for centrin and calmodulin.

To determine the temporal events that occur in this calcium binding protein during the H → D exchange perturbation, we have chosen to study the spectral region of 1500−1700 cm^{-1} in further detail. First, we temporally separated the spectral data that were acquired into two data sets: (1) the initial times (0−70 min) shown in Figure 4 and (2) the latter times of exchange (70−150 min) shown in Figure 5. Second, in a domain specific manner, we related the dynamics and solvation effects observed in Ccen-N and Ccen-C with the full-length protein. Auto peak positions determined from the synchronous plots (Figures 4A,C,E and 5A,C,E) and correlation peaks determined from the asynchronous plots (Figures 4B,D,F and 5B,D,F) at initial and latter times of exchange are summarized in Tables 1 and 2, respectively. Good agreement was observed for all three centrin samples. These band assignments and positions will be used to describe the dynamics of exchange observed for centrin.

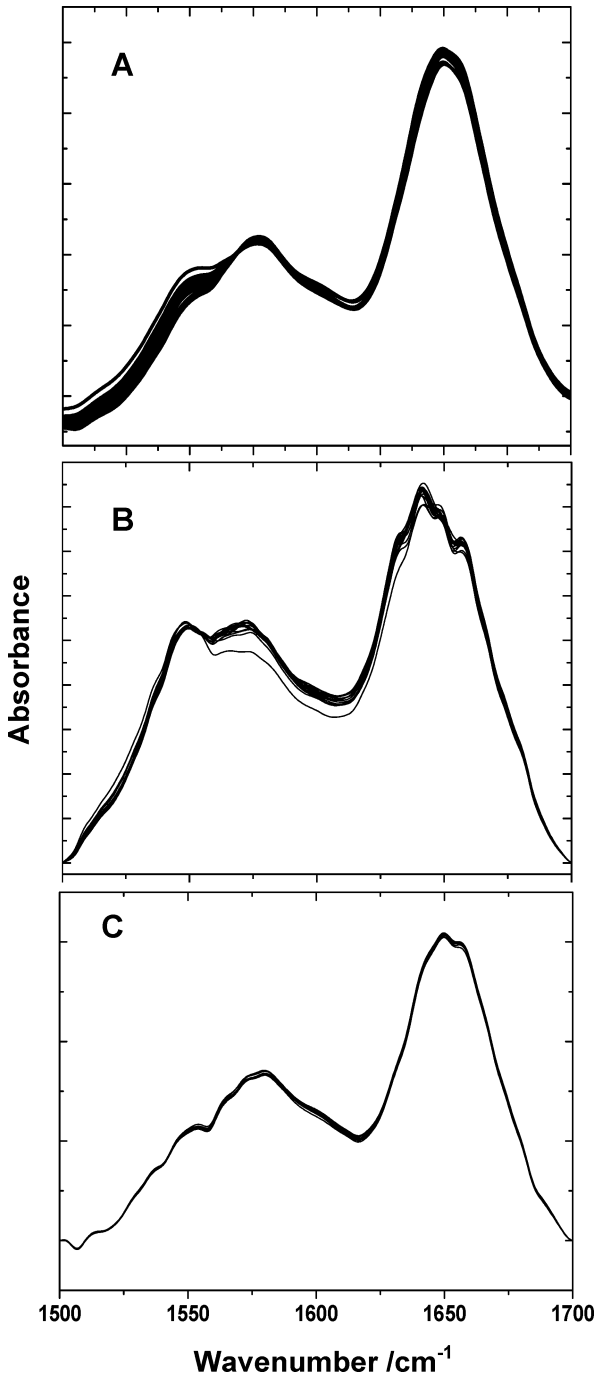

FIGURE 3: Overlaid spectra of *Chlamydomonas* centrin during H → D exchange in the spectral region of 1500−1700 cm^{-1}, at 20 °C for (A) the full-length centrin, (B) Ccen-N, and (C) Ccen-C. The spectral features that are shown are overlapped amide I and amide I′ bands and the amide II band comprised of side chain modes and N−H deformation mode.

During the first 70 min of H → D exchange for full-length centrin summarized in Table 3 and Figure 4B, the loop (1678 cm^{-1}) exchanges prior to the amino terminus (1560 cm^{-1}). The amino terminus (1560 cm^{-1}) and tyrosine hydroxyl group (1522 cm^{-1}) found in helix A exchange at similar rates prior to the α-helix (1646 cm^{-1}). The arginine side chains (1600 cm^{-1}) also exchange prior to the α-helix (1646 cm^{-1}). At latter times of exchange (70−140 min), summarized in Table 3 and Figure 5B, similar dynamics were observed: the loop (1670 cm^{-1}) exchanges prior to the Tyr (1510 cm^{-1}) and Arg residues (1580 and 1604 cm^{-1}) followed by the α-helix (1650 cm^{-1}). The *β*-strands were not observed, suggesting little or no exchange.

To validate the results obtained for the full-length protein, we have used the isolated domain constructs (Ccen-N and Ccen-C) of *Chlamydomonas* centrin. This enabled further understanding of the dynamics of exchange in centrin and allowed us to discriminate among the differences in solvation exchange dynamics in the helix, *β*-strand, and loop motifs within the protein.

Ccen-N. The dynamics of exchange at initial times (0−70 min) and at later times (70−150 min) are summarized in Table 4 and Figures 4D and 5D . At initial times, the amino terminus (1570 cm^{-1}) and tyrosine residue (1511 and 1520 cm^{-1}), in helix A, exchange first, followed by the *β*-strand (1630 cm^{-1}). The arginine residues (1592 and 1605 cm^{-1}) exchanged prior to the α-helix (1644 cm^{-1}). As a last step, in the initial times was the exchange of the loop (1666 cm^{-1}). During the latter times (70−150 min), the following dynamics of exchange were observed: *β*-strand (1638 cm^{-1}) exchanged prior to arginine (1578 and 1604 cm^{-1}) followed by α-helix (1645 cm^{-1}) and loop (1666 cm^{-1}).

Ccen-C. Similar dynamics in Ccen-C were observed for the initial and latter times. The loop (1666 cm^{-1}) exchanged first, followed by the α-helix (1640 cm^{-1}), and as a final step, the *β*-strand (1630 cm^{-1}) undergoes amide proton exchange. During the latter times, the loop (1670 cm^{-1}) exchanges prior to the α-helix (1650 cm^{-1}) and finally the *β*-strand (1634 cm^{-1}). In Ccen-C, two different helices (1640 cm^{-1} at initial times and 1650 cm^{-1} at latter times) were observed, suggesting different solvated states.

In summary, the dynamics of exchange of the loop and the helical structural motifs are different in the N-terminal domain when compared to those in the C-terminal domain. Also, the *β*-strand motifs were observed to exchange in the terminal domain fragments, providing key dynamic information in the overall exchange process. The results also suggest that self-association occurs in the carboxyl terminal end of centrin. The H → D exchange of arginine residues in Ccen-C could also be directly compared with that of arginine residues in calmodulin, suggesting differences in solvation and self-association of Ccen-C and the carboxyl-terminal end of full-length centrin.

Simulation of FT-IR Spectra Using Curve Fit Analysis. Curve fitting methods that are based on the two-dimensional analysis allow for the simulation of the two-dimensional plots obtained experimentally and can be used to verify interpretations of the experimental spectra. Panels A−C of Figure 6 represent the typical curve fit analysis for the fully exchanged sample. The simulated band positions were those obtained from the auto peaks of the synchronous plots summarized in Table 2 and described in an earlier publication (*21*). This approach was used because the dynamic spectral data obtained in H → D exchange experiments will only include vibrational modes that contain exchangeable protons. These exchangeable protons would include amides found in the backbone, amino terminus, and exchangeable side chain protons such as arginine primary amines and the tyrosine hydroxyl group. Therefore, the glutamates and aspartates observed in the one-dimensional spectra would not be observed in the two-dimensional correlational analysis plots. The simulation of full-length Ccen (results not shown) agrees well with the experimental data and confirms the correlation

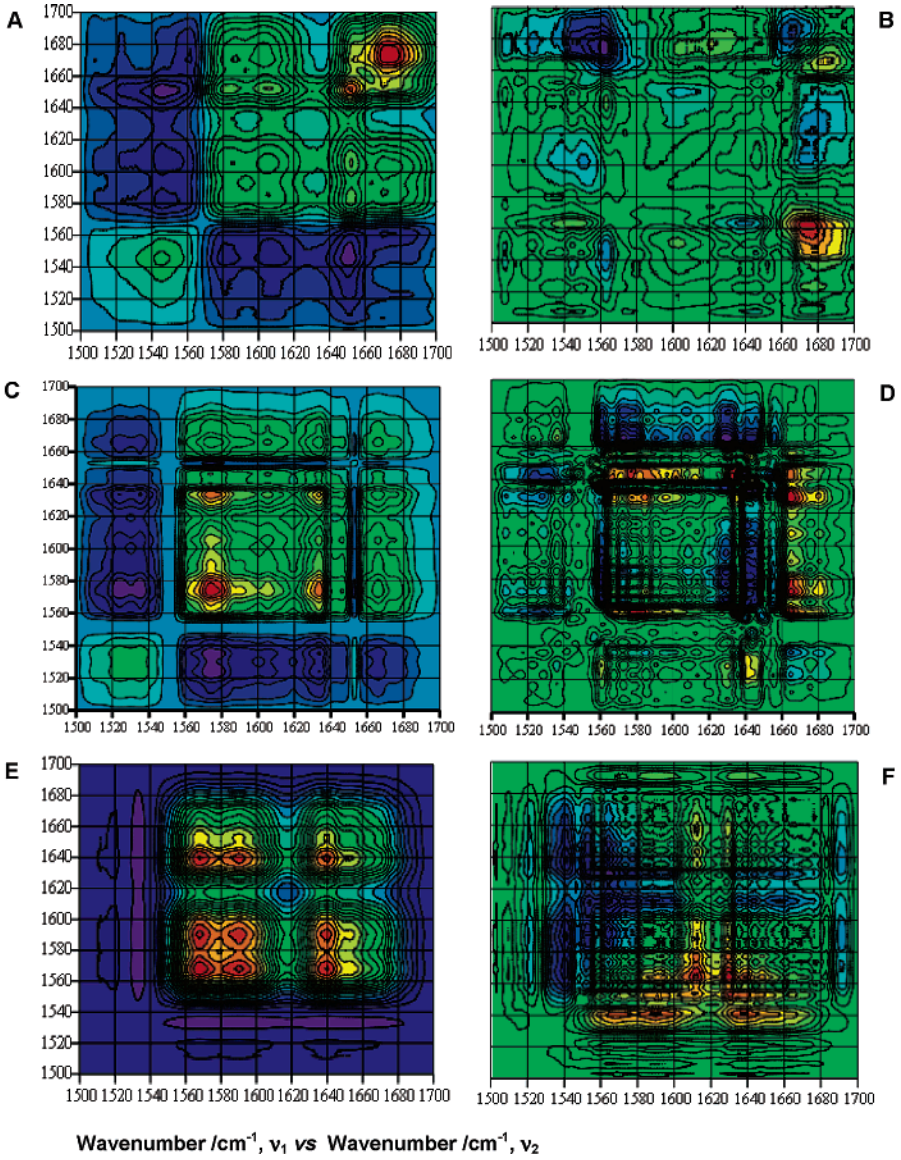

FIGURE 4: Two-dimensional correlational plots for *Chlamydomonas* centrin at initial times of H → D exchange (0−70 min) for the full-length protein [(A) synchronous and (B) asynchronous], Ccen-N [(C) synchronous and (D) asynchronous], and Ccen-C [(E) synchronous and (F) asynchronous].

between the arginine modes (1580 and 1606 cm^{-1}) and the loops (1680 cm^{-1}) or α-helix mode (1646 cm^{-1}).

Comparison of H → D Exchange Kinetics. By assuming that the decrease in the intensity of the amide II band is exclusively due to the exchange of the amide protons, the plot of the amide II/amide I intensity ratio as a function of time (Figure 7) shows H → D kinetics for (cyan spheres) full-length CaM, (maroon spheres) full-length Ccen, (○) Ccen-N, and (Θ) Ccen-C. The time interval over which exchange occurs can be related to the vibrational modes that are being affected by the chemical perturbation observed in the two-dimensional correlational plots shown in Figures 4 and 5. Specifically, the resulting kinetic curve observed for Ccen-N (○) plateaus after the first 20 min of the exchange process, while Ccen-C (Θ) has a slower decay curve which plateaus after 100 min. Full-length centrin (maroon spheres) has two different rates of exchange for the amide protons; the biphasic exchange process can be attributed to the contributions from the two independent domains. In contrast, CaM (cyan spheres) is observed to exchange within the first 20 min, suggesting different solvation dynamics.

DISCUSSION

Detailed study of the solvent exchange kinetics is not possible because of the unknown molar extinction for the carboxylate side chains (Asp^- and Glu^-) in the calcium binding site when coordinated with Ca^{2+} or Mg^{2+}. These contributions must be subtracted before detailed kinetic analysis is possible.

The method of spectral analysis used herein has proven to be successful in determining the dynamics of H → D exchange of this calcium binding protein and in theory can be used on any protein. Temporal dynamics of exchange for full-length centrin were as follows: the α-helix (1646 cm^{-1}) exchanged first, followed by the amino terminus and arginine modes, followed by the calcium binding loops. In full-length centrin, the Tyr residue exchanges within the first ~80 min, suggesting that this region of the helix is less accessible to

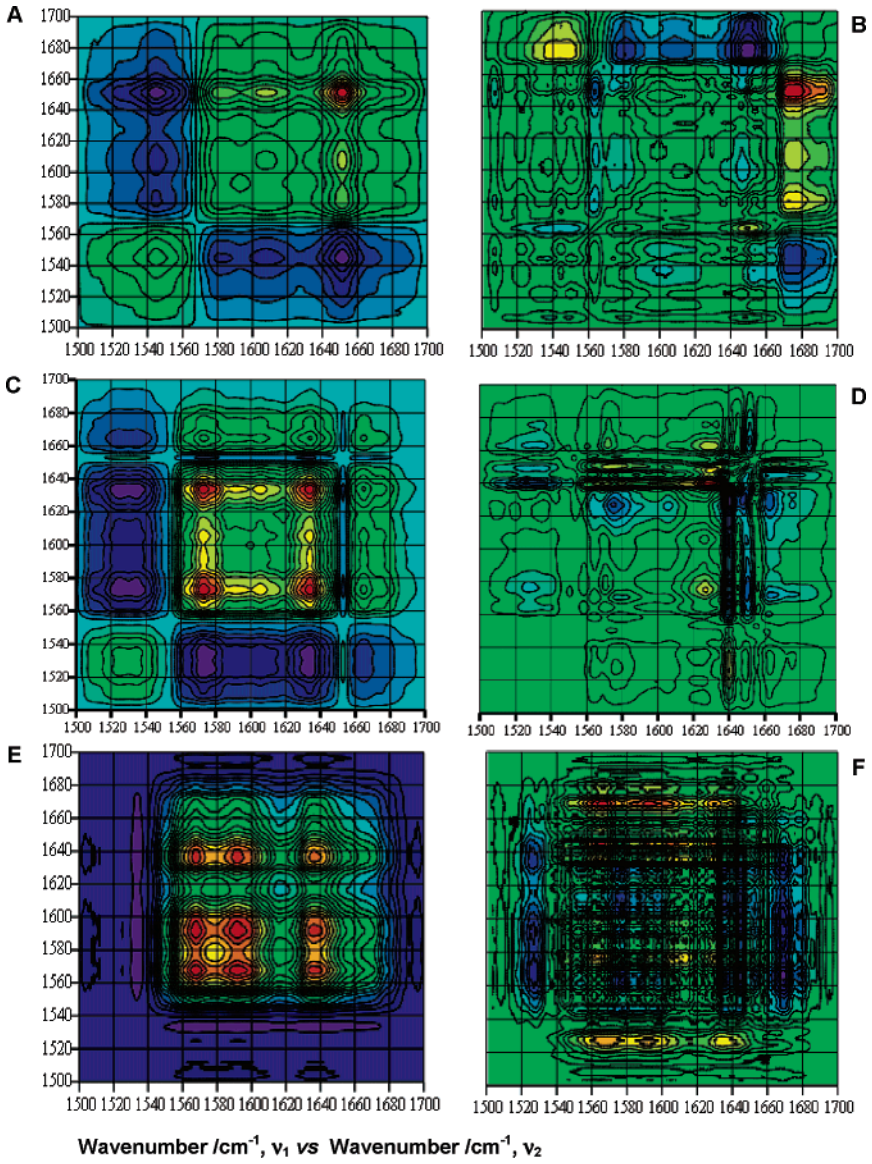

FIGURE 5: Two-dimensional correlational plots for *Chlamydomonas* centrin at later times of H → D exchange (70−150 min) for the full-length protein [(A) synchronous and (B) asynchronous], Ccen-N [(C) synchronous and (D) asynchronous], and Ccen-C [(E) synchronous and (F) asynchronous].

Table 1: Auto Peak Assignment from Two-Dimensional Correlation Analysis Plots Obtained for Initial Times (0−70 min) of H → D Exchange in the FT-IR Spectral Region of 1500−1700 cm^{-1}

	full length centrin		Ccen-N		Ccen-C	
assignment	synchronous (cm^{-1})	asynchronous (cm^{-1})	synchronous (cm^{-1})	asynchronous (cm^{-1})	synchronous (cm^{-1})	asynchronous (cm^{-1})
Tyr			1510	1511		
Tyr	1520	1522	1524	1520		
N−H deformation	1546	1544	1538	1538	1548	1540
amino terminus	1560	1560	1574	1570	1570	1566
Arg	1580	1580	1594	1592	1590	1590
Arg	1606	1600	1600	1605	1600	1604
β-strand			1636	1630		1630
α-helix			1646	1644	1640	1640
α-helix	1648	1646			1652	1650
β-turn (loop)	1676	1678	1665	1666	1670	1666

its aqueous environment. The tyrosine residue located in position 3 served as an internal probe for monitoring the H → D exchange dynamics at the amino-terminal end of helix A within centrin. During the latter times of exchange, arginine residues continue to exchange followed by loop amide protons and the remaining α-helical motifs (1650 cm^{-1}), which are less accessible to the aqueous environment. Meanwhile, for calmodulin, the exchange occurs first in the loops, then in the arginine residues, and finally in the helices. These arginine residues are located almost exclusively at the carboxyl-terminal end of CaM and exchange within the first 20 min, suggesting that these residues are exposed when

Table 2: Auto Peak Assignment from Two-Dimensional Correlation Analysis Plots Obtained for Later Times (70−150 min) of H → D Exchange in the FT-IR Spectral Region of 1500−1700 cm^{-1}

	full-length centrin		Ccen-N		Ccen-C	
assignment	synchronous (cm^{-1})	asynchronous (cm^{-1})	synchronous (cm^{-1})	asynchronous (cm^{-1})	synchronous (cm^{-1})	asynchronous (cm^{-1})
Tyr	1510	1510	1510	1511		
Tyr	1524	1522	1522	1520		
N−H deformation	1546	1544	1536	1536	1550	1544
amino terminus	1560	1560	1564	1560	1568	1568
Arg	1580	1580	1574	1578	1590	1592
Arg	1608	1604	1600	1604	1606	1610
β-strand			1636	1638	1636	1634
α-helix	1652	1650	1648	1645	1654	1650
β-turn (loop)	1670	1670	1666	1666	1670	1670

Table 3: Summary of Phase Analysis Used To Determine Hydrogen−Deuterium Exchange Dynamics in Full-Length *Chlamydomonas* Centrin within 0−150 min

event[a]	asynchronous plot analysis[b]
1	loop (1678 cm^{-1}) prior to Arg (1600 cm^{-1})
2	N−H deformation (1546 cm^{-1}) prior to Arg (1600 cm^{-1})
3[c]	loop (1678 cm^{-1}) prior to amino terminus and Tyr (1560 and 1522 cm^{-1}, respectively)
4[c]	amino terminus and Tyr (1560 and 1522 cm^{-1}, respectively) prior to Arg (1600 cm^{-1})
5[c]	amino terminus and Tyr (1560 and 1522 cm^{-1}, respectively) prior to α-helix (1646 cm^{-1})
6	Arg (1600 cm^{-1}) prior to α-helix (1646 cm^{-1})
7	loop (1670 cm^{-1}) prior to α-helix (1646 cm^{-1})
8[c]	loop (1670 cm^{-1}) prior to Tyr (1522 cm^{-1})
9[c]	Tyr (1522 cm^{-1}) prior to Arg (1604 cm^{-1})
10	loop (1678 cm^{-1}) prior to Arg (1580 and 1604 cm^{-1})
11[c]	Tyr (1522 cm^{-1}) prior to α-helix (1646 cm^{-1})
12	N−H deformation (1546 cm^{-1}) prior to Arg (1580 and 1604 cm^{-1})
13[c]	amino terminus and Tyr (1560 and 1522 cm^{-1}, respectively) prior to N−H deformation (1546 cm^{-1})

[a] Events 1−6 comprise the initial times of exchange (0−70 min), and events 7−13 comprise the latter times of exchange (70−150 min). [b] Peak assignment and cross-peak positions have been used to describe each event. [c] The amino-terminal end and a single Tyr residue located only in helix A.

Table 4: Summary of Phase Analysis Used To Determine Hydrogen−Deuterium Exchange Dynamics in Ccen-N within 0−150 min

event[a]	asynchronous plot analysis[b]
1	loop (1666 cm^{-1}) prior to α-helix (1644 cm^{-1})
2	loop (1666 cm^{-1}) prior to Arg (1592 and 1605 cm^{-1})
3[c]	loop (1666 cm^{-1}) prior to amino terminus (1574 cm^{-1}) and Tyr (1510 cm^{-1})
4	Arg (1592 and 1605 cm^{-1}) prior to β-strand (1630 cm^{-1})
5[c]	amino terminus (1574 cm^{-1}) and Tyr (1510 cm^{-1}) prior to β-strand (1630 cm^{-1})
6	loop (1666 cm^{-1}) prior to β-strand (1630 cm^{-1})
7	α-helix (1644 cm^{-1}) prior to β-strand (1630 cm^{-1})
8	β-strand (1638 cm^{-1}) prior to loop (1666 cm^{-1})
9	β-strand (1638 cm^{-1}) prior to Arg (1578 and 1604 cm^{-1})
10	Arg (1578 and 1604 cm^{-1}) prior to loop (1666 cm^{-1})
11	α-helix (1645 cm^{-1}) prior to β-strand (1638 cm^{-1})
12	β-strand (1638 cm^{-1}) prior to α-helix (1645 cm^{-1})
13	N−H deformation (1536 cm^{-1}) prior to Arg (1578 and 1604 cm^{-1})
14	N−H deformation (1536 cm^{-1}) prior to loop (1666 cm^{-1})
15	N−H deformation (1536 cm^{-1}) prior α-helix (1645 cm^{-1})
16	α-helix (1645 cm^{-1}) prior to N−H deformation (1536 cm^{-1})

[a] Events 1−7 comprise the initials times of exchange (0−70 min), and events 7−16 comprise the latter times of exchange (70−150 min). [b] Peak assignment and cross-peak positions have been used to describe each event. [c] A single tyrosine residue located in helix A.

Table 5: Summary of Phase Analysis Used To Determine Hydrogen−Deuterium Exchange Dynamics in Ccen-C within 0−150 min

event[a]	asynchronous plot analysis[b]
1	loop (1666 cm^{-1}) prior to Arg (1590 and 1604 cm^{-1})
2	N−H deformation (1540 cm^{-1}) prior to Arg (1590 and 1604 cm^{-1})
3	amino terminus (1566 cm^{-1}, helix E) prior to Arg (1590 and 1604 cm^{-1})
4	loop (1666 cm^{-1}) prior to α-helix (1640 cm^{-1})
5	loop (1666 cm^{-1}) prior to β-strand (1630 cm^{-1})
6	loop (1670 cm^{-1}) prior to Arg (1592 and 1610 cm^{-1})
7	N−H deformation (1544 cm^{-1}) prior to Arg (1592 and 1610 cm^{-1})
8	Arg (1592 and 1610 cm^{-1}) prior to amino terminus (1568 cm^{-1}, helix E)
9	loop (1670 cm^{-1}) prior to α-helix (1650 cm^{-1})
10	Arg (1592 cm^{-1}) prior to β-strand (1634 cm^{-1})
11	loop (1670 cm^{-1}) prior to β-strand (1634 cm^{-1})
12	N−H deformation (1544 cm^{-1}) prior to β-strand (1634 cm^{-1})

[a] Events 1−5 comprise the initials times of exchange (0−70 min), and events 6−12 comprise the latter times of exchange (70−150 min). [b] Peak assignment and cross-peak positions have been used to describe each event.

compared to Ccen-C. The α-helices (1640 and 1650 cm^{-1}) observed in this study show two different environments, reflecting differences in the degree of exposure of the amides to their aqueous environment. This lower-frequency shift of the exposed helices results from the amide carbonyl bond stretch vibrational mode weakening, due to the deuterium bonding from the solvent. In addition, the arginine side chain mode has also served as an internal probe, and these residues are found in the helices and are indicators of the extent of solvation of the helices.

Domain specific dynamics were obtained by studying the isolated domain under the same conditions that were used for the full-length protein. The amino terminus and tyrosine

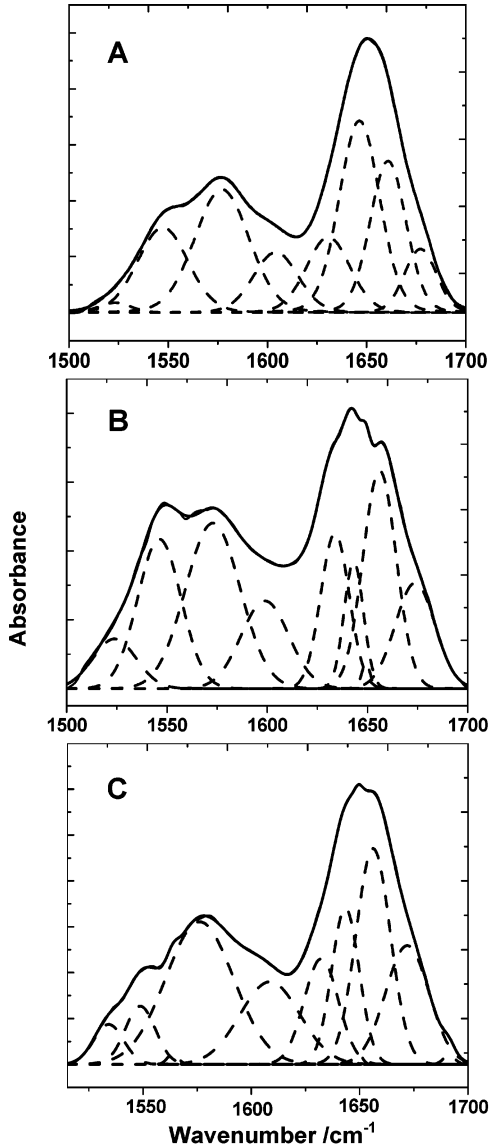

FIGURE 6: Typical curve-fit spectra of *Chlamydomonas* centrin fully exchanged in the spectral region of 1400−1700 cm^{-1}: (A) full-length centrin, (B) Ccen-N, and (C) Ccen-C. All subbands used for the curve fit have been assigned to a vibrational mode.

residue, located in helix A, exchange prior to the helix amide protons (1644 cm^{-1}) in Ccen-N, suggesting helix A is more exposed to its aqueous environment when compared to its full-length counterpart. This event was followed by the β-strand and then Arg side chain exchange and finally the α-helix and loop amide protons. For Ccen-C, exchange dynamics involves the amino terminus (helix E) first and then loops followed by the arginine residues. Once the arginine exchanges, then the α-helix (1650 cm^{-1}) amide protons and β-strands are observed to exchange as the last steps. The β-strands are not observed to exchange in full-length centrin, and this may be due to solvation differences in the full-length centrin when compared to the isolated domains or weak intensity changes for the β-strand vibrational mode in the spectrum.

Chlamydomonas centrin was observed to have differences in helix solvation in its two domains; in contrast, calmodulin differences in solvation were not observed. This observation is relevant to the biochemistry of centrin since the C-terminal domain, but not the N-terminal domain, has been found to

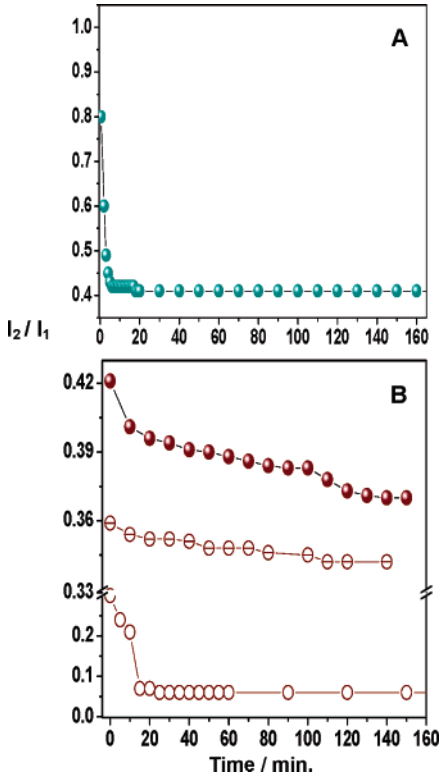

FIGURE 7: Typical exponential decay curves during H → D exchange using the integrated amide II/amide I intensity ratios for (cyan spheres) full-length CaM, (maroon spheres) full-length Ccen, (○) the amino-terminal domain (Ccen-N), and (Θ) the carboxy-terminal domain (Ccen-C).

interact with specific targets (*38*, *39*). Holocentrin has been found to self-associate at the carboxy-terminal domain (manuscript in preparation). Therefore, the α-helix (1650 cm^{-1}) found exclusively in the carboxy-terminal domain, which is less exposed to its aqueous environment and has slower rates of H → D exchange, may be due to its self-association. The internal probes (Arg and Tyr) provided additional information about temporal events during H → D exchange that could be assigned to specific regions within the protein. These provided further information about the extent of solvation in the helical structural motifs within Ccen-N and Ccen-C.

The biophysical study on centrin solvation dynamics discussed herein provides further evidence of the structural independence of the domains. These in vitro studies are the groundwork for comparison with complexes of centrin, its terminal domain fragments, and other interacting proteins and peptides such as Kar1p, Mps3p, and, most recently discovered, sfi1p, involved in the duplication and assembly of spindle pole body (SPB) (*13*, *16*, *17*). This last protein, sfi1p, has been found to have up to 23 centrin binding sites, which have affinity for centrin at low calcium concentrations. In contrast, Kar1p and mps3p have been found to interact with centrin at higher calcium concentrations. Future H → D exchange dynamic studies will involve the study of these complexes in providing insight into the biochemical changes by which centrin plays a role in the process of cell division.

ACKNOWLEDGMENT

We thank Dr. Mike Holmes for the mass spectral analysis used to verify centrin's purity at the Protein Core Facility at

the Mayo Clinic and Foundation. We also thank Gisselle Román for the FT-IR spectral acquisition of calmodulin.

REFERENCES

1. Nakayama, S., Moncrief, N. D., and Kretsinger, R. H. (1992) Evolution of EF-hand calcium-modulated proteins. II. Domains of several subfamilies have diverse evolutionary histories, *J. Mol. Evol. 34*, 416−448.
2. Kawasaki, H., Nakayama, S., and Kretsinger, R. H. (1998) Classification and evolution of EF-hand proteins, *BioMetals 11*, 277−295.
3. Weber, C., Lee, V. D., Chazin, W. J., and Huang, B. (1994) High-Level Expression in *Escherichia-Coli* and Characterization of the EF-hand Calcium-Binding Protein Caltractin, *J. Biol. Chem. 269*, 15795−15802.
4. Veeraraghavan, S., Fagan, P. A., Hu, H., Lee, V., Harper, J. F., Huang, B., and Chazin, W. J. (2002) Structural Independence of the Two EF-hand Domains of Caltractin, *J. Biol. Chem. 277*, 28564−28571.
5. Hartman, H., and Fedorov, A. (2002) The origin of the eukaryotic cell: A genomic investigation, *Proc. Natl. Acad. Sci. U.S.A. 99*, 1420−1425.
6. Salisbury, J. L. (1989) Centrin and The Algal Flagellar Apparatus, *J. Phycol. 25*, 201−206.
7. Levy, Y. Y., Lai, E. Y., Remillard, S. P., Heintzelman, M. B., and Fulton, C. (1996) Centrin is a conserved protein that forms diverse associations with centrioles and MTOCs in *Naegleria* and other organisms, *Cell Motil. Cytoskeleton 33*, 298−323.
8. Salisbury, J. L. (1998) Roots, *J. Eukaryotic Microbiol. 45*, 28−32.
9. Salisbury, J. L. (1989) Alga Centrin: Calcium-sensitive Contractile Organelles. Algal Centrin, *Algae as Experimental Systems*; Alan R. Liss Inc.: New York; pp 19−37.
10. Salisbury, J. L. (1995) Centrin, centrosomes, and mitotic spindle poles, *Curr. Opin. Cell Biol. 7*, 39−45.
11. Schiebel, E., and Bornens, M. (1995) In search of a function for centrins, *Trends Cell Biol. 5*, 197−201.
12. Baum, P., Furlong, C., and Byers, B. (1986) Yeast gene required for spindle pole body duplication: Homology of its product with Ca^{2+}-binding proteins, *Proc. Natl. Acad. Sci. U.S.A. 83*, 5512−5516.
13. Jaspersen, S. L., Giddings, T. H., Jr., and Winey, M. (2002) Mps3p is a novel component of the yeast spindle pole body that interacts with the yeast centrin homologue Cdc31p, *J. Cell Biol. 159*, 945−956.
14. Salisbury, J. L., Suino, K., Busby, R., Delva, E., and D'Assoro, A. B. (2002) Knockdown of Centrin-2 arrests centriole duplication and activates a centrosome-based cell cycle checkpoint, *Mol. Biol. Cell 13*, 50A.
15. Salisbury, J. L., Suino, K. M., Busby, R., and Springett, M. (2002) Centrin-2 is required for centriole duplication in mammalian cells, *Curr. Biol. 12*, 1287−1292.
16. Kilmartin, J. V. (2003) Sfi1p has conserved centrin-binding sites and an essential function in budding yeast spindle pole body duplication, *J. Cell Biol. 162*, 1211−1221.
17. Salisbury, J. L. (2004) Centrosomes: Sfi1p and centrin unravel a structural riddle, *Curr. Biol. 14*, R27−R29.
18. White, R. A., Pan, Z., and Salisbury, J. L. (2000) GFP-centrin as a marker for centriole dynamics in living cells, *Microsc. Res. Tech. 49*, 451−457.
19. Marshall, W. F., and Rosenbaum, J. L. (2000) How centrioles work: Lessons from green yeast, *Curr. Opin. Cell Biol. 12*, 119−125.
20. Marshall, W. F. (2001) Centrioles take center stage, *Curr. Biol. 11*, R487−R496.
21. Pastrana-Rios, B., Ocana, W., Rios, M., Vargas, G. L., Ysa, G., Poynter, G., Tapia, J., and Salisbury, J. L. (2002). Centrin: Its secondary structure in the presence and absence of cations, *Biochemistry 41*, 6911−6919.
22. Pastrana-Rios, B., Sanoguet, Z., and Ocaña, W. (2002) Secondary structure changes in a calcium binding protein: centrin, *Sci. World J. 2*, 62−64.
23. Wiech, H., Geier, B. M., Paschke, T., Spang, A., Grein, K., Steinkotter, J., Melkonian, M., and Schiebel, E. (1996) Characterization of green alga, yeast, and human centrins: Specific subdomain features determine functional diversity, *J. Biol. Chem. 271*, 22453−22461.
24. Krimm, S., and Bandekar, J. (1986) Vibrational Spectroscopy and Conformation of Peptides, Polipeptides, and Proteins, *Adv. Protein Chem. 38*, 181−364.
25. Arrondo, J. L. R., Muga, A., Castresana, J., and Goñi, F. M. (1993) Quantitative Studies of the Structure of Proteins in Solution by Fourier Transform Infrared Spectroscopy, *Prog. Biophys. Mol. Biol. 59*, 23−56.
26. Graff, D. K., Pastrana-Rios, B., Venyaminov, S. Y., and Prendergast, F. G. (1997) The effects of chain length and thermal denaturation on helix-forming peptides: A mode-specific analysis using 2D FT-IR, *J. Am. Chem. Soc. 119*, 11282−11294.
27. Pastrana-Rios, B. (2001) Mechanism of unfolding of a model helical peptide, *Biochemistry 40*, 9074−9081.
28. de Jongh, H. H., Goormaghtigh, E., and Ruysschaert, J. M. (1997) Amide-proton exchange of water-soluble proteins of different structural classes studied at the submolecular level by infrared spectroscopy, *Biochemistry 36*, 13603−13610.
29. Nabet, A., and Pezólet, M. (1997) Two-dimensional FT-IR spectroscopy: A powerful method to study the secondary structure of proteins using H−D exchange, *Appl. Spectrosc. 51*, 466−469.
30. Raussens, V., Ruysschaert, J. M., and Goormaghtigh, E. (2004) Analysis of $^1H/^2H$ exchange kinetics using model infrared spectra, *Appl. Spectrosc. 58*, 68−82.
31. Vigano, C., Smeyers, M., Raussens, V., Scheirlinckx, F., Ruysschaert, J. M., and Goormaghtigh, E. (2004) Hydrogen−deuterium exchange in membrane proteins monitored by IR spectroscopy: A new tool to resolve protein structure and dynamics, *Biopolymers 74*, 19−26.
32. Noda, I. (1989) Two-Dimensional Infrared (2D IR) Spectroscopy: Theory and Applications, *Appl. Spectrosc. 44*, 550−560.
33. Noda, I., Dowrey, A. E., Marcott, C., Story, G. M., and Ozaki, Y. (2000) Generalized two-dimensional correlation spectroscopy, *Appl. Spectrosc. 54*, 236A−248A.
34. Ozaki, Y., Murayama, K., Wu, Y., and Czarnik-Matusewicz, B. (2003) Two-dimensional infrared correlation spectroscopy studies on secondary structures and hydrogen bondings of side chains of proteins, *Spectrosc. Int. J. 17*, 79−100.
35. Goormaghtigh, E., Raussens, V., and Ruysschaert, J. M. (1999) Attenuated total reflection infrared spectroscopy of proteins and lipids in biological membranes, *Biochim. Biophys. Acta 1422*, 105−185.
36. Arrondo, J. L. R., and Goni, F. M. (1999) Structure and dynamics of membrane proteins as studied by infrared spectroscopy, *Prog. Biophys. Mol. Biol. 72*, 367−405.
37. Chirgadze, Y. N., Fedorov, V., and Trushina, N. P. (1975) Estimation of Amino Acid Residue Side-chain Absorption in the Infrared Spectra of Protein Solutions in Heavy Water, *Biopolymers 14*, 679−694.
38. Durussel, I., Blouquit, Y., Middendorp, S., Craescu, C. T., and Cox, J. A. (2000) Calcium, *FEBS Lett. 472*, 208−212.
39. Hu, H., and Chazin, W. J. (2003) Unique features in the C-terminal domain provide caltractin with target specificity, *J. Mol. Biol. 330*, 473−484.

BI0484419